RSC Advances

This is an *Accepted Manuscript*, which has been through the Royal Society of Chemistry peer review process and has been accepted for publication.

Accepted Manuscripts are published online shortly after acceptance, before technical editing, formatting and proof reading. Using this free service, authors can make their results available to the community, in citable form, before we publish the edited article. This *Accepted Manuscript* will be replaced by the edited, formatted and paginated article as soon as this is available.

You can find more information about *Accepted Manuscripts* in the Information for Authors.

Please note that technical editing may introduce minor changes to the text and/or graphics, which may alter content. The journal's standard Terms & Conditions and the Ethical guidelines still apply. In no event shall the Royal Society of Chemistry be held responsible for any errors or omissions in this *Accepted Manuscript* or any consequences arising from the use of any information it contains.

ROYAL SOCIETY OF CHEMISTRY

www.rsc.org/advances

Please do not adjust margins

Journal Name

ARTICLE

Electrodeposition of PtNi bimetallic nanoparticles on three-dimensional graphene for highly efficient methanol oxidation

Received 00th January 20xx,
Accepted 00th January 20xx

DOI: 10.1039/x0xx00000x

www.rsc.org/

Ruiping Xiu, Feifei Zhang*, Zonghua Wang*, Min Yang, Jianfei Xia, Rijun Gui and Yanzhi Xia

In the present work, platinum-nickel (PtNi) bimetallic nanoparticles with a uniform diameter of 40 nm were anchored onto a three-dimensional graphene (3DGN) by using the method of electrodeposition. The resulting PtNi/3DGN composites were developed toward highly active catalysts for methanol oxidation. Experimental results revealed that the PtNi/3DGN composites exhibited improved electrocatalytic capacity (the forward anodic peak current density of 822.1 mA/mg_{Pt} in methanol oxidation when compared with Pt alone (251.2 mA/mg_{Pt}) and Pt/3DGN (416.9 mA/mg_{Pt}), and indicated the high tolerance to carbon monoxide generated in the process of methanol oxidation.

Introduction

The direct methanol fuel cell (DMFC), a fascinating factory to convert chemical energy of methanol into electrical energy, has attracted considerable interests due to its high energy density, low operating temperature, less pollutant emission and quick start-up[1-3]. However, the commercialization of DMFC is hindered by sluggish oxidation reaction of methanol, and high cost and easy deactivation of platinum (Pt) catalysts[4-8]. To improve the electrocatalytic activity of Pt catalysts for methanol oxidation, some modified approaches have been developed typically, including controlling morphology and facets of Pt nanoparticles[9-13]; alloying it with other transition metals such as Ru, Ni, Pd and Ag[14-18]; as well as supporting Pt based nanocatalysts onto supports such as carbon black[19], carbon nanotube[20], mesoporous carbon[21] and garphene[22].

The addition of a second metal improves the surface chemistry and reactivity properties of Pt, and based on the bi-functional mechanism[23-25] and ligand electronic effect[26-29], the alloying strategy is promising. In previous reports, the PtNi catalysts exhibited a higher activity and a better tolerance to carbon monoxide (CO) poisoning, when compared with the pure Pt[24, 30]. Additionally, the alloying of PtNi can reduce the demand of precious metal Pt. Nickel (Ni) alloying with Pt can reduce the electronic binding energy of Pt, which contributes to the methanol oxidation. Nickel oxides in PtNi bimetallic catalysts provide the oxidation of CO at lower potentials with an oxygen source[31].

An appropriate support with a large surface area, high electrical conductivity and good stability, could promises a high dispersion of Pt or Pt-based alloying nanoparticles and the maximum utilization of noble materials[32, 33]. Graphene, a two-dimensional carbon material with fully delocalized π-electrons, is extensively used as an excellent supporting material because of its extremely large surface area, high charge carrier mobility, good mechanical stiffness, and chemical and thermal stability[34-39]. However, the strong planar stacking of two-dimensional graphene nanosheets leads to a serious deterioration of properties due to the formation of irreversible agglomerates during electrode assembly[40, 41]. Recently, great efforts have been devoted to preparing three-dimensional graphene (3DGN) nanostructures, so as to extending the excellent properties of graphene into its three-dimensional structure and in the meanwhile overcoming the restacking of two-dimensional graphene[42-44]. The large porous architecture of 3DGN maximizes the surface area availability of catalysts, and the resulting catalysts exhibit a better mass transport of reactants for the applications of fuel cell[45-47].

In the present work, PtNi/3DGN composites were prepared by electrodepositon technology and further developed as the catalyst for methanol oxidation. The three-dimensional architecture of 3DGN contributed to the uniform dispersion of PtNi nanoparticles and provided a large mass and electron transport kinetics for the catalytic reaction. Relative efforts in this work focused on the achievement of catalysts with improved electrocatalytic activity, good capacity of anti-CO poisoning and high stability for methanol oxidation.

Experimental

Reagents and apparatus

College of Chemical Science and Technology, Laboratory of Fiber Materials and Modern Textile, the Growing Base for State Key Laboratory, Shandong Sino-Japanese Center for Collaborative Research of Carbon Nanomaterials, Collaborative Innovation Center for Marine Biomass Fiber Materials and Textiles, Qingdao University, Qingdao, Shandong 266071, China. E-mail: wangzonghua@qdu.edu.cn; zhangfeifei00921@163.com;
Tel and Fax: + 86-532-85950873
Electronic Supplementary Information (ESI) available. See: DOI: 10.1039/x0xx00000x

RSC Advances Accepted Manuscript

Graphite was provided by Qingdao Fujin graphite Corp., Ltd., China). $H_2PtCl_6 \cdot 6H_2O$, $Ni(NO_3)_2 \cdot 6H_2O$, CH_3OH and H_2SO_4 were purchased from Sinopharm Chemical Reagent Co. Ltd.(Shanghai, China). All the reagents were of analytical grade and used without further purification. Doubly distilled water was employed throughout the experiment.SEM images were taken by JEOL JSM-6500F equipped with an energy dispersive X-ray spectrometry (EDS) and TEM images taken by JEOL JEM-2100.The structural analysis of the as-prepared catalysts were investigated by X-ray diffraction (XRD, DX2700, China) operating with Cu Kα radition (λ = 1.5418Å). Cyclic voltammetry (CV) and chronoamperometry measurements were conducted on a CHI 660C electrochemical workstation (Shanghai, China) with a conventional three-electrode system. A glassy carbon electrode (GCE, 3 mm in diameter) was used as the working electrode, while saturated calomel electrode (SCE) and a Pt foil were used as the reference electrode and the counter electrode, respectively. All potentials reported in this work were with respect to the SCE reference electrode.

Preparation of PtNi/3DGN nanocomposite

The graphene oxide (GO) was synthesized by using a modified Hummers method[48]. Typically, 60 mL of GO aqueous solution (2 mg/mL) was placed into a Teflon-lined autoclave and heated to 180°C keeping for 6h[49]. After repeatedly washing with distilled water and following freeze-drying treatment, 3DGN was obtained successfully. Then, 1 mg of 3DGN was ultrasonically dispersed in the mixture of 1 mL of ethanol and 20 µL of Nafion solution (5wt.%) to generate a homogeneous black suspension. After that, 6 µL of the suspension was dropped onto a GCE and dried at room temperature (forming 3DGN/GCE).Finally, the as-prepared 3DGN/GCE was immersed in the mixed aqueous solution of 0.1 M of $Ni(NO_3)_2$ plus 0.038 M of H_2PtCl_6, and the corresponding cyclic scan in the potential range from -0.8 V to 1.2 V was performed (Fig. 1) to obtain PtNi/3DGN composite catalysts. The reduction peak at 0.25 V was attributed to $PtCl_6^{2-}$reduction and the reduction peak at -0.59 V was due to Ni^{2+} reduction. The preparation procedures of Pt/3DGN catalysts were similar to that of PtNi/3DGN in the absence of $Ni(NO_3)_2$. Pt catalysts were prepared by immersing GCE in 0.038 M of $H_2PtCl_6$and scanning in the potential range of -0.8 to 1.2V.The effective surface area of GCE for deposition is 0.07 cm^2. The loadings of Pt in Pt, Pt/3DGN and PtNi/3DGN catalysts are calculated with values of 9.2 µg, 11.5 µg and 10.0 µg, respectively.

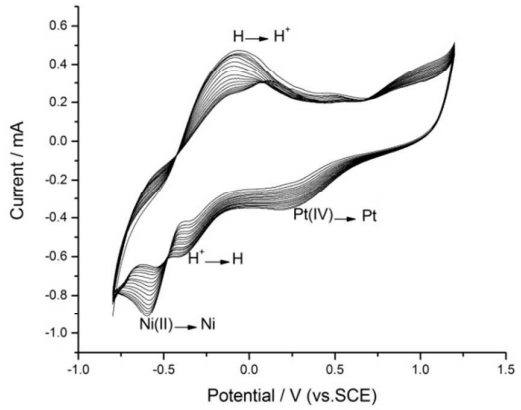

Fig. 1 CVs of 3DGN/GCE in 0.1 M $Ni(NO_3)_2$ +0.038 M H_2PtCl_6 at a scan rate of 100mV/s, number of potential cycles: 20.

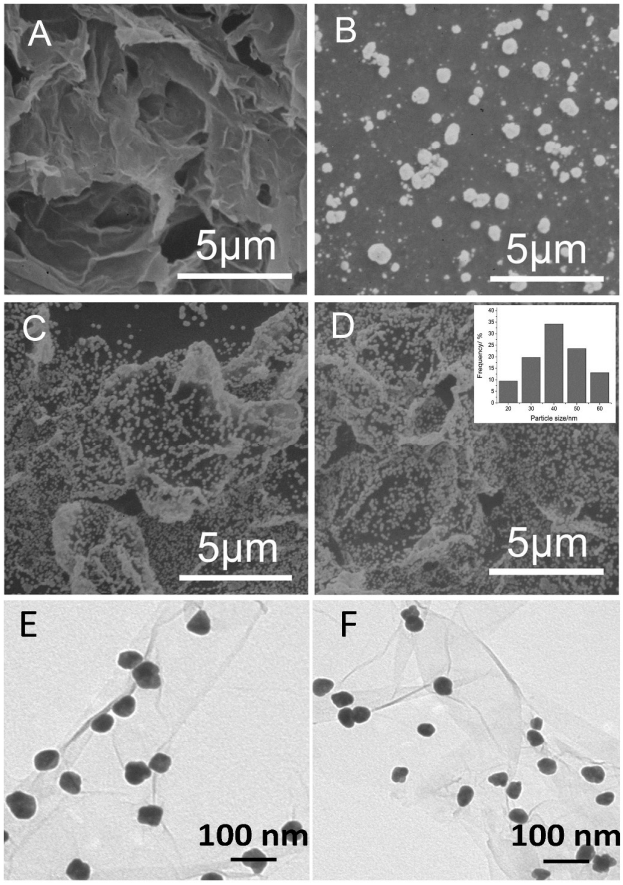

Fig. 2 SEM images of 3DGN (A), Pt (B), Pt/3DGN (C) and PtNi/3DGN (D). Insert is the histogram of particle size distribution for PtNi/3DGN; TEM images of Pt/3DGN (E) and PtNi/3DGN (F).

RSC Advances Accepted Manuscript

 This journal is © The Royal Society of Chemistry 20xx

Results and discussion

Morphological characterization

SEM images in Fig. 2 depict the morphology and structure of as-prepared products. As indicated in Fig. 2A and Fig. S1 (A), the prepared 3DGN represents an interconnected three-dimensional porous frameworks and multi-wrinkles. The Raman spectra of GO and 3DGN were shown in Fig. S1 (B), displaying two peaks around 1345 cm^{-1} and 1585 cm^{-1} corresponding to the D and G bands, respectively. The D band is related to structural defects in the curved graphene sheet or partially disordered structures of graphitic domains, while the G band corresponds to the graphitic hexagon-pinch pattern. The D/G intensity ratio increases from GO to 3DGN, which is due to the defects introduced into the 3DGN during reduction[50, 51].

The three-dimensional structures enable the good mechanical properties of graphene, and provide sufficient binding sites of graphene for PtNi nanoparticles to anchor. As observed, the PtNi nanoparticles can homogeneously anchored on the 3DGN by an electrodeposition process, thus exhibited better defined morphologies and smaller diameters (Fig.2D) than Pt nanoparticles supported on the GCE (Fig. 2B). Pt/3DGN (Fig. 2C) shown similar particle distribution with PtNi/3DGN (Fig. 2D). The PtNi nanoparticles anchored on 3DGN have an average diameter of 40 nm, which is smaller than that of Pt (~90 nm, Fig. S2(A)) and Pt/3DGN (~55 nm, Fig. S2(B)), respectively. The decreased diameter and uniformly distribution of PtNi nanoparticles could be attributed to the delocalized π-electrons and three-dimensional porous frameworks of 3DGN, which significantly enlarge the accessible surface area for electrodepositon. The composition of PtNi/3DGN composite was estimated by EDS (shown in Fig.S3), revealing the presence of C, O, Pt and Ni, further demonstrating that the PtNi nanoparticles were deposited on 3DGN.Based on the EDS spectra, the atomic ratio of Pt/Ni is about 2:1.

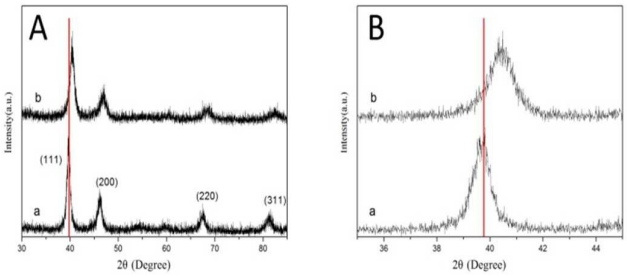

Fig. 3(A) XRD patterns of Pt/3DGN (a) and PtNi/3DGN (b); (B) Pt (111) peak in Pt/3DGN (a) and PtNi/3DGN (b).

Fig. 3 gives the XRD patterns of Pt/3DGN and PtNi/3DGN. In the case of Pt/3DGN (Fig. 3A (a)), the peaks around 39.8, 46.5, 67.5 and 81.5 correspond to the (111), (200), (220) and (311) planes of Pt face-centered cubic (fcc) crystal structure (JCPDS 04-0802), respectively, indicating that there is a formation of fcc-crystal structured Pt on 3DGN. For the PtNi/3DGN (Fig. 3A (b)), diffraction patterns show the same peaks as mentioned above. However, the diffraction peaks slightly shift to higher angle than that of Pt/3DGN. The minor shift of the Pt peaks is account for that Ni atom has come into the Pt lattice with the alloy formation between Pt and Ni[28, 52].

Electrochemical characterization

Fig. 4shows the CVs of GCE coated with different electrocatalysts in 1 M of H_2SO_4 at a scan rate of 100mV/s. In the electrochemical process, H_2 adsorption-desorption is used to describe the electrochemically surface area (ECSA) of catalysts, which indirectly evaluates the catalyst available active sites for electrons transferred to and from the electrode. The ECSA of catalysts is calculated from Fig.4 by measuring the charge gained in the H_2 adsorption-desorption region after double-layer correction, in which a value of 210 $\mu C/cm^2$ is assumed for the adsorption of a hydrogen monolayer[53]. The ECSA of PtNi/3DGN (c, 87.4m^2/g_{Pt}) is larger than that of Pt (a, 20.7m^2/g_{Pt}) and Pt/3DGN (b, 53.8m^2/g_{Pt}). Combination of Fig. 2 is further evidence for the improved dispersion and small diameter of PtNi nanoparticles anchoring on 3DGN.

Cyclic scan for methanol oxidation was performed in 1 M of H_2SO_4 and 1 M of CH_3OH aqueous solution containing Pt (a) catalysts, Pt/3DGN (b) and PtNi/3DGN (c) composite catalysts, respectively (Fig. 5). The measurements were conducted with the potential range of -0.2to 1.2 V at a voltage scan rate of 100 mV/s. Pt (a), Pt/3DGN (b) and PtNi/3DGN (c) catalysts show similar trends that there are well-separated anodic peaks in the forward scan (I_f) and the backward scan (I_b), which characterize the process of methanol oxidation. The forward peak magnitude is depended on the amount of methanol oxidized at the electrode modified by catalysts. The backward peak is originated from the removal of CO and the oxidation of other intermediate carbonaceous species. PtNi/3DGN (c, 822.1 mA/mg_{Pt}) showed a higher current density of oxidation reaction for methanol when compared with Pt(a, 251.2 mA/mg_{Pt}) and Pt/3DGN (b, 416.9 mA/mg_{Pt}). In addition, the ratios of I_f/I_b are determined to be 1.87 for PtNi/3DGN (c), 1.52 for Pt/3DGN (b) and 1.23 for Pt (a), respectively. These results indicated that methanol molecules adsorbed on PtNi/3DGN could be much oxidized during the forward scan and form relatively few poisonous carbonaceous species. Furthermore, PtNi/3DGN (c) exhibited a more negative onset potential than that of Pt (a). The larger surface area and the increased active adsorption sites accelerated reaction rate and avoided the accumulation of carbonaceous intermediates, thus resulting in the improved catalytic activity and high resistance to CO poisoning. Also, the addition of Ni, based on the bi-functional mechanism[23-25] and ligand electronic effect[26-29], improves the

RSC Advances Accepted Manuscript

surface chemistry and reactivity properties of Pt which contributed to the catalytic ability for methanol oxidation.

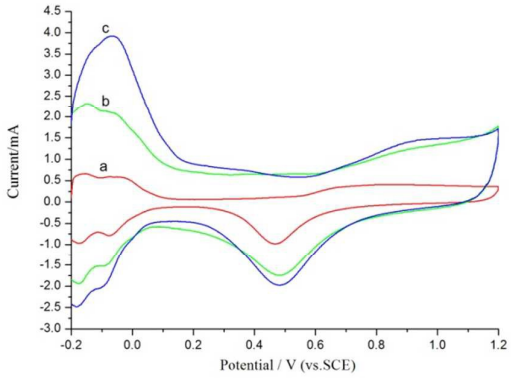

Fig. 4 CVs of Pt (a), Pt/3DGN (b) and PtNi/3DGN (c) in the solution of 1.0 mol/L H_2SO_4 at a scan rate of 100mV/s

As exhibited in Fig. 6, the chronoamperometric curves of Pt (a) Pt/3DGN (b) and PtNi/3DGN (c) were measured in the aqueous solution of 1 M H_2SO_4 and 1 M CH_3OH at 0.65 V to investigate the catalytic activities and the electrochemical stabilities of catalysts. The current density for methanol oxidation exhibited a rapid decay at the initial stage for Pt (a), Pt/3DGN (b) and PtNi/3DGN (c), which may result from the formation of carbonaceous intermediates. After several minutes, the current density decreased slowly and reached a steady state. PtNi/3DGN (c) composite catalyst exhibited a lower degradation rate and a higher steady state current density than those of Pt (a) and Pt/3DGN (b). Thus, the PtNi/3DGN catalyst demonstrated a superior catalytic activity and electrochemical stability. These results should be ascribed to the bi-functional mechanism and ligand electronic effect of PtNi bimetallic catalysts and the unique three-dimensional structure of 3DGN which facilitates the effective loading and uniform distribution of PtNi nanoparticles. To further evaluate the performance of our prepared PtNi/3DGN catalyst, some relevant reported works have been generalized in Table 1 for comparison. Comparably speaking, our catalyst PtNi/3DGN shows less CO tolerance than PtRu/VG[15], which can be considered as a disadvantage. However, it displays relatively higher performance for the catalytic activity and CO tolerance compared to some of the other reported works. So, more intensive and targeted research is deserved to pursue more significant performance.

Table 1

Comparison of our work with other relevant reported works on the catalytic activity for methanol oxidation

Catalyst	ECSA (m^2/g_{Pt})	Mass activity (mA/mg_{Pt})	I_f/I_b	References
Pt-CeO_2/graphene	66.4	440.1	1.48	54
Pt/PB/graphene	85.7	445	1.37	37
PtNi/graphene	98	413	1.33	52
PtPd NW/RGO	23.0	510	1.29	16
Pt_{24}/RGO	36.7	550.4	1.24	39
Pt-Ru/VG	—	339.2	3.3	15
Pt/3DGN	53.8	416.9	1.52	this work
PtNi/3DGN	87.4	822.1	1.87	this work

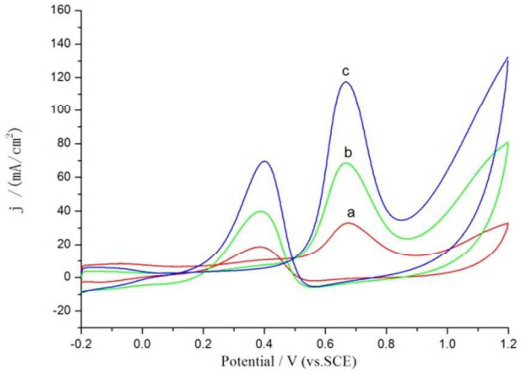

Fig. 5 CVs of Pt (a), Pt/3DGN (b) and PtNi/3DGN (c) in the solution of 1 mol/L H_2SO_4 containing 1 mol/L CH_3OH at a scan rate of 100mV/s

RSC Advances Accepted Manuscript

This journal is © The Royal Society of Chemistry 20xx

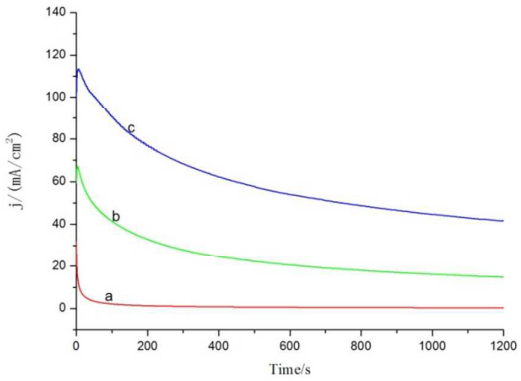

Fig. 6 Chronoamperometric curves for Pt (a), Pt/3DGN (b) and PtNi/3DGN (c) in the solution of 1 mol/L H_2SO_4 containing 1 mol/L CH_3OH at a fixed potential of 0.65 V vs. SCE (KCl sat.).

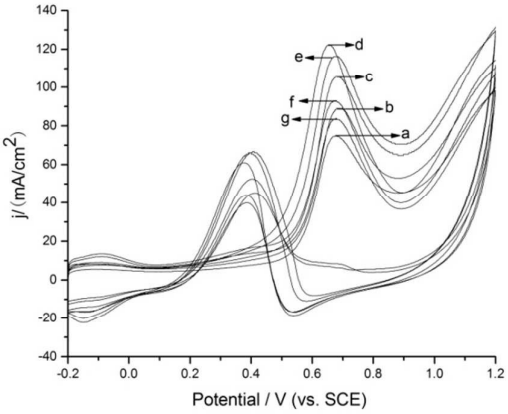

Fig. 7 CVs of PtNi/3DGN in the solution of H_2SO_4 containing 1 mol/L CH_3OH at a scan rate of 100 mV/s, the concentration of H_2SO_4(mol/L): a) 0.4，b) 0.6，c) 0.8，d)1.0，e) 1.2，f) 1.4，g) 1.6

Optimization of parameters

In Fig. 7, the cyclic voltammograms of PtNi/3DGN at different concentrations of H_2SO_4 were recorded in 1 M of methanol with the potential range of -0.2 to 1.2 V at a scan rate of 100 mV/s. As observed, the anodic current density increased with the increase of H_2SO_4 concentrations and leveled off at concentrations higher than 1.0 M. The increase of H^+ concentration (less than 1 M) contributed to the conductivity of the solution, so accelerating the reaction rate. When the concentration of H^+ was higher than 1 M, the negative effect was assumed to be caused by the saturation of H^+ in solution, which impeded the breaking of C-H in methanol oxidation[55-57]. In accordance with this result, the optimum concentration of H_2SO_4 was close to 1 M.

Fig. 8A displays electrocatalytic behavior of PtNi/3DGN for methanol oxidation at different scan rates by cyclic voltammetry in 1 M H_2SO_4 and 1 M CH_3OH solution. As can be seen from Fig. 8B, the peak current density exhibited a linear relation versus the square root of the scan rate with R of 0.9983, revealing that the electrocatalytic process is controlled by diffusion.

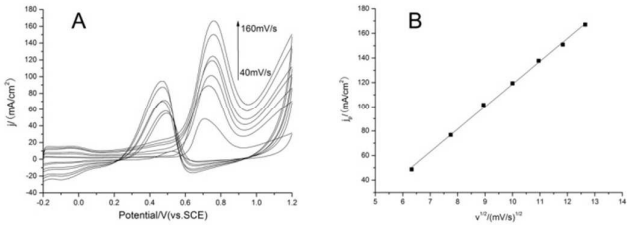

Fig. 8 (A) CVs of the PtNi/3DGN catalyst in the solution of 1mol/L H_2SO_4 containing 1mol/L CH_3OH. Scan rate: 40, 60, 80, 100, 120, 140, 160 mV/s follow the arrow; (B) the variation of the peak current density in the positive sweeping with the square root of scanning rate.

Conclusions

The novel PtNi/3DGN composite catalysts consisting of PtNi bimetallic nanoparticles anchored on 3DGN were fabricated by electrodeposition method. Experimental results revealed that PtNi nanoparticles were uniformly distributed on the porous 3DGN. The as-prepared PtNi/3DGN composite catalysts exhibited excellent electrocatalytic activity, high tolerance to CO poisoning and good stability. The PtNi/3DGN composites as anode catalyst exhibited a significantly improved reaction rate for methanol oxidation.

Acknowledgements

We really appreciate the financial support from the National Natural Science Foundation of China (21405086, 21275082, 81102411, 21203228 and 21475071), the National Key Basic Research Development Program of China (973 special preliminary study plan, Grant no.: 2012CB722705), the Taishan

RSC Advances Accepted Manuscript

Scholar Program of Shandong Province, the Natural Science Foundation of Shandong (2014BSB01552, ZR2011BQ005, and BS2014NJ023) and the Natural Science Foundation of Qingdao (13-1-4-128-jch and 13-1-4-202-jch).

Notes and references

1. E. Reddington, A. Sapienza, B. Gurau, R. Viswanathan, S. Sarangapani, E. S. Smotkin and T. E. Mallouk, *Science*, 1998, **280**, 1735-1737.
2. M. V. Martinez-Huerta, J. L. Rodriguez, N. Tsiouvaras, M. A. Pena, J. L. G. Fierro and E. Pastor, *Chem. Mater.*, 2008, **20**, 4249-4259.
3. C. Q. Wang, F. F. Ren, C. Y. Zhai, K. Zhang, B. B. Yang, D. A. Bin, H. W. Wang, P. Yang and Y. K. Du, *Rsc Adv.*, 2014, **4**, 57600-57607.
4. G. Mpourmpakis, A. N. Andriotis and D. G. Vlachos, *Nano Lett.*, 2010, **10**, 1041-1045.
5. H. M. Sun, L. Y. Cao and L. H. Lu, *Acta Chim. Sinica*, 2013, **71**, 579-584.
6. H. C. He, P. Xiao, M. Zhou, F. L. Liu, S. J. Yu, L. Qiao and Y. H. Zhang, *Electrochi. Acta*, 2013, **88**, 782-789.
7. Y. Tong, J. Pu, H. Y. Wang, S. B. Wang, C. Liu and Z. H. Wang, *J. Electroanal. Chem.*, 2014, **728**, 66-71.
8. A. Nouralishahi, A. M. Rashidi, Y. Mortazavi, A. A. Khodadadi and M. Choolaei, *Appl. Surf. Sci.*, 2015, **335**, 55-64.
9. Y. Sun, L. Zhuang, J. Lu, X. Hong and P. Liu, *J. Am. Chem. Soc.*, 2007, **129**, 15465-15467.
10. H. Q. Ji, M. G. Li, Y. L. Wang and F. Gao, *Electrochem. Commun.*, 2012, **24**, 17-20.
11. M. Yaldagard, M. Jahanshahi and N. Seghatoleslami, *Appl. Surf. Sci.*, 2014, **317**, 496-504.
12. B. Y. Xia, H. B. Wu, Y. Yan, H. B. Wang and X. Wang, *Small*, 2014, **10**, 2336-2339.
13. Z. Luo, L. Yuwen, B. Bao, J. Tian, X. Zhu, L. Weng and L. Wang, *J. Mater. Chem.*, 2012, **22**, 7791-7796.
14. G. H. An and H. J. Ahn, *J. Electroanal. Chem.*, 2013, **707**, 74-77.
15. Z. Bo, D. Hu, J. Kong, J. H. Yan and K. F. Cen, *J. Power Sources*, 2015, **273**, 530-537.
16. S. F. Du, Y. X. Lu and R. Steinberger-Wilckens, *Carbon*, 2014, **79**, 346-353.
17. L. Li, Y. Wu, J. Lu, C. Nan and Y. Li, *Chem. Commun.*, 2013, **49**, 7486-7488.
18. J. Y. Cao, M. W. Guo, J. Y. Wu, J. Xu, W. C. Wang and Z. D. Chen, *J. Power Sources*, 2015, **277**, 155-160.
19. X. Huang, Z. Zhao, Y. Chen, E. Zhu, M. Li, X. Duan and Y. Huang, *Energy Environ. Sci.*, 2014, **7**, 2957-2962.
20. Y. Mu, H. Liang, J. Hu, L. Jiang and L. Wan, *J. Phys. Chem. B*, 2005, **109**, 22212-22216.
21. T. Maiyalagan, T. O. Alaje and K. Scott, *J. Phys. Chem. C*, 2012, **116**, 2630-2638.
22. L. Hong, Y. Hao, Y. Yang, J. Yuan and L. Niu, *Nanotechnology*, 2015, **26**, 045604.
23. M. Watanabe and S. Motoo, *Journal of Electroanalytical Chemistry and Interfacial Electrochemistry*, 1975, **60**, 267-273.
24. H. Yang, C. Coutanceau, J. M. Leger, N. Alonso-Vante and C. Lamy, *J. Electroanal. Chem.*, 2005, **576**, 305-313.
25. M. C. Denis, M. Lefevre, D. Guay and J. P. Dodelet, *Electrochim. Acta*, 2008, **53**, 5142-5154.
26. T. Toda, H. Igarashi, H. Uchida and M. Watanabe, *J. Electrochem. Soc.*, 1999, **146**, 3750-3756.
27. C. Lu, C. Rice, R. I. Masel, P. K. Babu, P. Waszczuk, H. S. Kim, E. Oldfield and A. Wieckowski, *J. Phys. Chem. B*, 2002, **106**, 9581-9589.
28. K. W. Park, J. H. Choi, B. K. Kwon, S. A. Lee, Y. E. Sung, H. Y. Ha, S. A. Hong, H. Kim and A. Wieckowski, *J. Phys. Chem. B*, 2002, **106**, 1869-1877.
29. M. K. Jeon, J. Y. Won, K. R. Lee and S. I. Woo, *Electrochem. Commun.*, 2007, **9**, 2163-2166.
30. X. J. Liu, C. H. Cui, M. Gong, H. H. Li, Y. Xue, F. J. Fan and S. H. Yu, *Chem. Commun.*, 2013, **49**, 8704-8706.
31. Y. Zhao, Y. F. E, L. Z. Fan, Y. F. Qiu and S. H. Yang, *Electrochim. Acta*, 2007, **52**, 5873-5878.
32. J. S. Yu, S. Kang, S. B. Yoon and G. Chai, *J. Am. Chem. Soc.*, 2002, **124**, 9382-9383.
33. E. Antolini and E. R. Gonzalez, *Appl. Catal.A:Gen.*, 2009, **365**, 1-19.
34. P. P. Yao, P. L. Chen, L. Jiang, H. P. Zhao, H. F. Zhu, D. Zhou, W. P. Hu, B. H. Han and M. H. Liu, *Adv. Mate.*, 2010, **22**, 5008-+.
35. S. J. Guo, S. J. Dong and E. K. Wang, *Acs Nano*, 2010, **4**, 547-555.
36. S. J. Guo and S. J. Dong, *Chem. Soc. Rev.*, 2011, **40**, 2644-2672.
37. Z. H. Wang, G. Y. Shi, J. F. Xia, Y. Z. Xia, F. F. Zhang, L. Xia, D. M. Song, J. Q. Liu, Y. H. Li, L. H. Xia and M. E. Brito, *Electrochim. Acta*, 2014, **121**, 245-252.
38. V. Singh, D. Joung, L. Zhai, S. Das, S. I. Khondaker and S. Seal, *Prog. Mater. Sci.*, 2011, **56**, 1178-1271.
39. L.-N. Zhou, X.-T. Zhang, W.-J. Shen, S.-G. Sun and Y.-J. Li, *RSC Adv.*, 2015, **5**, 46017-46025.
40. C.-C. Kung, P.-Y. Lin, Y. Xue, R. Akolkar, L. Dai, X. Yu and C.-C. Liu, *J. Power Sources*, 2014, **256**, 329-335.
41. Z. H. Wang, G. Y. Shi, F. F. Zhang, J. F. Xia, R. J. Gui, M. Yang, S. Bi, L. Xia, Y. H. Li, L. H. Xia and Y. Z. Xia, *Electrochim. Acta*, 2015, **160**, 288-295.
42. Z. S. Wu, Y. Sun, Y. Z. Tan, S. B. Yang, X. L. Feng and K. Mullen, *J. Am. Chem. Soc.*, 2012, **134**, 19532-19535.
43. S. H. Lee, H. W. Kim, J. O. Hwang, W. J. Lee, J. Kwon, C. W. Bielawski, R. S. Ruoff and S. O. Kim, *Angew. Chem. Int. Ed.*, 2010, **49**, 10084-10088.
44. Q. Zhang, F. X. Jiang, R. R. Yue and Y. K. Du, *Rsc Adv.*, 2014, **4**, 12105-12108.
45. Y. C. Yong, X. C. Dong, M. B. Chan-Park, H. Song and P. Chen, *Acs Nano*, 2012, **6**, 2394-2400.
46. S. Y. Yin, Y. Y. Zhang, J. H. Kong, C. J. Zou, C. M. Li, X. H. Lu, J. Ma, F. Y. C. Boey and X. D. Chen, *Acs Nano*, 2011, **5**, 3831-3838.
47. Z. H. Tang, S. L. Shen, J. Zhuang and X. Wang, *Angew. Chem. Int. Ed.*, 2010, **49**, 4603-4607.
48. Z. Wang, Q. Han, J. Xia, L. Xia, M. Ding and J. Tang, *J. Sep. Sci.*, 2013, **36**, 1834-1842.
49. Y. X. Xu, K. X. Sheng, C. Li and G. Q. Shi, *ACS Nano*, 2010, **4**, 4324-4330.
50. H.-L. Guo, X.-F. Wang, Q.-Y. Qian, F.-B. Wang and X.-H. Xia, *ACS Nano*, 2009, **3**, 2653-2659.
51. Z. Wang, G. Shi, F. Zhang, J. Xia, R. Gui, M. Yang, S. Bi, L. Xia, Y. Li, L. Xia and Y. Xia, *Electrochim. Acta*, 2015, **160**, 288-295.
52. Y. Hu, P. Wu, H. Zhang and C. Cai, *Electrochim. Acta*, 2012, **85**, 314-321.
53. Z. Yan, H. Wang, M. Zhang, Z. Jiang, T. Jiang and J. Xie, *Electrochim. Acta*, 2013, **95**, 218-224.
54. S. Yu, Q. Liu, W. Yang, K. Han, Z. Wang and H. Zhu, *Electrochim. Acta*, 2013, **94**, 245-251.
55. A. Hamnett, *Catal. Today*, 1997, **38**, 445-457.
56. M. Baldauf and W. Preidel, *J. Power Sources*, 1999, **84**, 161-166.
57. Y. Huang, S. Zheng, X. Lin, L. Su and Y. Guo, *Electrochim. Acta*, 2012, **63**, 346-353.

RSC Advances Accepted Manuscript

 This journal is © The Royal Society of Chemistry 20xx

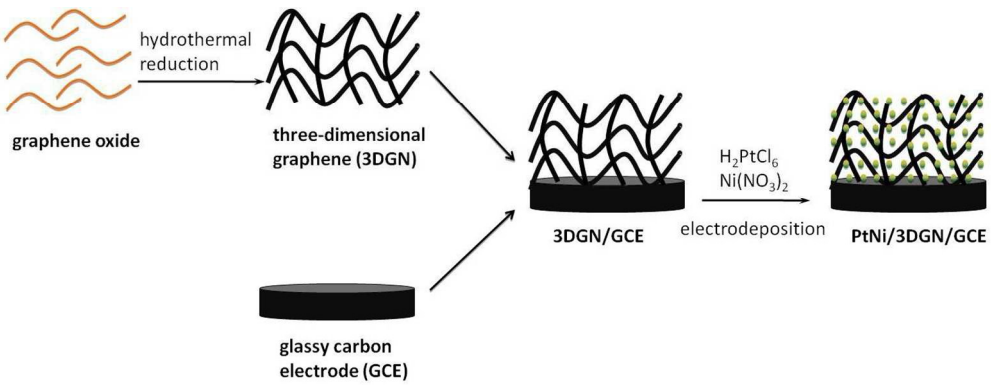

314x120mm (120 x 120 DPI)

RSC Advances Accepted Manuscript